J Mater Sci (2017) 52:6506–6524

Sequestration of methylene blue (MB) dyes from aqueous solution using polyaniline and polyaniline–nitroprusside composite

Ferooze Ahmad Rafiqi[1,*] and Kowsar Majid[1]

[1] *Department of Chemistry, National Institute of Technology Srinagar, Hazratbal, Srinagar, J&K 190006, India*

Received: 4 October 2016
Accepted: 3 February 2017
Published online: 9 February 2017

ABSTRACT

This paper reports polyaniline–nitroprusside (PANI–NP) composite prepared via in situ polymerization of polyaniline in the presence of sodium nitroprusside complex using ammonium persulphate oxidant. Comparison between the MB dye elimination from aqueous solution using polyaniline and polyaniline–nitroprusside composite is investigated with UV–visible spectroscopy. The maximum adsorption capacity for PANI and PANI–NP composite at 25 °C are 412.80 and 496.85 mg g^{-1}, respectively. About 80% removal of MB occurs in 1 h using pure PANI from (50 mg MB/100 mL) aqueous solution and 99.37% removal is observed in just 5 min, when PANI–NP composite is used. Adsorption kinetics is in good agreement with pseudo-first order for polyaniline and pseudo-second order for polyaniline–nitroprusside composite. The adsorption data fits well with the Langmuir model for both PANI and PANI–NP composite. Langmuir and Tempkin model suggests chemisorption type of interactions between the MB and adsorbents. Thermodynamic study revealed that the adsorption of MB on PANI and PANI–NP composite is exothermic and spontaneous in nature. Moreover, regeneration and reuse of PANI–NP composite as adsorbent is possible only at higher temperature. FTIR studies further confirm the successful adsorption of MB on PANI and PANI–NP composite. On the basis of vey short equilibrium adsorption time and very high adsorption capacity for MB dye, PANI–NP composite could be used as a most efficient adsorbent for the removal of cationic dyes from any real sample.

Introduction

With the growing demand of human civilization and mad race towards the industrialization and urbanization, dyes have received considerable attention. The emission of industrial effluents from the industries worldwide impinges a negative impact on all living forms due to their toxic and adverse effects. Dyes are used in industries like paper, rubber, plastic, medicine, concrete, cosmetics, food industries

Address correspondence to E-mail: feroozerafiqi@rediffmail.com; kowsarmajid@rediffmail.com

DOI 10.1007/s10853-017-0886-z

and the textile sector which is the most consumers of dyes [1, 2]. More than 90% of all the dyes in use are synthetic dyes [1]. The dyes are manufactured annually in tones and demand in the market is according to the colour and index [3]. In this work, we have chosen methylene blue (MB) dye as a test probe for remedial experiments. Albeit MB has lot of application and is mainly used as disinfector in dye stuffs and a colouring material in paper, temporary hair, cottons, wools and other textile items but its harmful effects cannot be ignored. It is reported to have some harmful effects in human beings such as cyanosis, jaundice, vomiting, tissue necrosis, heart-beat imbalance etc. [4]. In the past for the removal of dyes from waste water and industrial effluents, coagulation and flocculation, chemical reduction, advanced oxidative processes, ozonization, membrane separation, ultra-filtration and electro-precipitation techniques were used [3, 5]. These techniques were expensive, less efficient and not environment friendly. An alarming signal of clean water crises worldwide and its scarcity day by day due to repercussions of global warming calls for the attention of environment friendly new technologies, of which adsorption is the most extensive, cheap and efficient method to remove organic and inorganic toxins from the contaminated water.

Separation of undesirable moieties from the liquid phase by the adsorption process was tested with adsorbents like oxides, clay minerals, silica, graphene and activated carbon etc. [6–11] but 100% removal of pollutants has not been achieved so far. Conducting polymer composites are nowadays used and proved to be more efficient towards dye removal [12]. Among all the conducting polymers, PANI is the most efficient and widely used as an efficient adsorbent because of its unique chemistry [13]. Emeraldine salt of polyaniline is used for the removal of sulphonated dyes [14]. Polyaniline microspheres are also used for the removal of methyl orange from aqueous solution [15]. Polyaniline–chitosan composite is used not only for fluoride ion adsorption but also for the removal of sulphonated dyes [16]. Polyaniline–silica composite has been used for removal of Acid green dyes from aqueous solution [17]. Polyaniline surpasses other conducting polymers in many ways because of its good economics, environment friendly, high adsorption efficiency, three dimensional porous polymeric structure, protonation de-protonation tendency, redox properties, good charge carrier mobility, light weight, flexible nature etc. [18–22]. Because of its typical porous structure, it not only absorbs and retains water but also accelerates the diffusion of dye molecules throughout its body [23]. Polyaniline has protonic imine groups that can adsorb anionic dyes and lone pairs on nitrogens of amine groups are the driving force for cationic dye adsorption through electrostatic attraction. This makes the polyaniline a potent material for both cationic and anionic dye adsorption. This motivates us to synthesize a composite of PANI with a metal complex, sodium nitroprusside with the purpose to improve "its adsorption capability". The selection behind the use of sodium nitroprusside as a filler in the matrix of PANI is owing to its features like non-chelated nature, high negative charge density over the nitroprusside complex ion, large surface area and thermally stable complex besides being non toxic, easily available and a cheap chemical [24]. SNP has an octahedral geometry with $t_{2g}^6 e_g^0$ configuration [25]. Non-chelated complexes like nitroprusside and ferricyanide impart high negative charge density on the PANI backbone making it suitable for dye and heavy metal ion adsorption. In chelated complexes, lone pair of electrons present on ligands is used for complexation. Therefore no additional active sites are available on polyaniline composite for metal ion and dye molecule adsorption. This is the advantage of non-chelated complexes over the chelated ones. Sodium nitroprusside exists in two living metastable states which makes it useful as an optical memory storage material [26]. It is also used as a precursor in catalyzed redox reactions and a vasodilator [24]. These properties suggest a unique chemistry of sodium nitroprusside.

In this work, a polyaniline metal complex based composite is prepared via in situ oxidative polymerization method. To the best of our knowledge, this is the first time that such type of polymer composite based metal complex will be employed for the removal of MB from aqueous solution. The novelty of the work is in the achievement of almost 100% adsorption of MB onto this newly synthesized composite. The effects of contact time, adsorbent dosage, initial concentration of MB, pH and temperature are investigated. Moreover, the kinetic and thermodynamic parameters are evaluated.

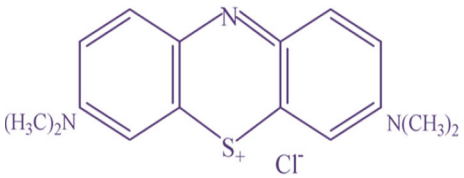

Figure 1 Structure of methylene blue (MB).

Experimental

Materials

Sodium nitroprusside $Na_2[Fe(CN)_5NO]$, methylene blue (MB) were of Merck quality. MB has the molecular formula $C_{16}H_{18}N_3SCl$ and the molecular structure is shown in Fig. 1. It is highly soluble in water and produces a blue coloured cationic dye dispersed in solution. Aniline is supplied by Loba chemicals and used after distillation. Ammonium persulphate $(NH_4)_2S_2O_8$ is also supplied by Loba chemicals. Hydrochloric acid (HCl) and NaOH are of analytical grade. Triply distilled water is used for the synthesis and adsorption experiments.

Instrument and measurements

The FTIR spectra were recorded on a Perkin-Elmer spectrometer using KBr pellets. XRD data was collected from PW 3050 base diffractometer with CuK_α radiation of 1.540598 Å. Ultraviolet–visible (UV–Vis) spectra were taken on double beam UV–visible spectrophotometer T 80 using a cell of 1 cm optical path length and wavelength range of 200–1000 nm. Surface area was determined by N_2 adsorption–desorption at 75 K with Brunauer–Emmet–Teller (BET) method using an ASAP 2420 System. Surface morphology of the samples was studied on Hitachi scanning electron microscope model S-3600N. The thermal analysis was carried out on a PerkinElmer thermal analyzer in N_2 atmosphere at a heating rate of 10 °C/min.

Synthesis

Synthesis of pure polyaniline (PANI)

Polyaniline was prepared by known methods of oxidation of aniline with ammonium persulphate $(NH_4)_2S_2O_8$ [27]. 7.5 g of $(NH_4)_2S_2O_8$ was dissolved in 180 mL of water. 3 mL of aniline was then added drop wise to this solution with continuous stirring. The mole ratio between ammonium persulphate and aniline was kept 1:1. The mixture was magnetically stirred for 3 h at 0–2 °C and was left for more than 1 h. The greenish black precipitate resulting from this solution was filtered and washed repeatedly with distilled water. The precipitate was collected and dried in an oven at 40 °C.

Synthesis of polyaniline–nitroprusside composite (PANI–$[Fe(CN)_5NO]$ composite)

7.5 g of $(NH_4)_2S_2O_8$ was dissolved in 190 mL of 1 M aqueous HCl solution. 3 mL of aniline was then added drop wise to this solution with continuous stirring. 2 g of sodium nitroprusside was added to the whole mixture solution. The reaction mixture was magnetically stirred for 3 h at 0–2 °C. The blue greenish precipitate obtained after filtration was washed with CH_3OH and then with distilled water. It was dried in an oven at 40 °C for 24 h. The dried sample was kept in a desiccator.

Adsorption experiments

To perform adsorption experiments, 50.5 mg of MB is dissolved in 50 mL aqueous solution and treated with 0.5 g of polyaniline and polyaniline–nitroprusside composite, separately. The solutions were agitated with magnetic stirrer with a rotating speed of 150 rpm for definite time intervals. At the end of predetermined time interval, simple filtration is used for the removal of adsorbent and then filtrate is analyzed for the unadsorbed MB, spectrophotometrically. Concentrations of MB at different time intervals are calculated using Lambert–Beer's Law represented by Eq. 1.

$$A = \varepsilon bc \tag{1}$$

where A is absorbance, b is thickness of the cell, ε is molar extinction coefficient which is a constant for a particular species at a particular temperature and c is concentration of the MB in the solution.

Results and discussion

XRD characterization

X-ray diffraction (XRD) analysis were conducted on PW-3050 base diffractometer with CuK_α radiations (scanning range 2θ: 2.5°–60°). Figure 2a–c shows the XRD pattern of Sodium Nitroprusside (SNP),

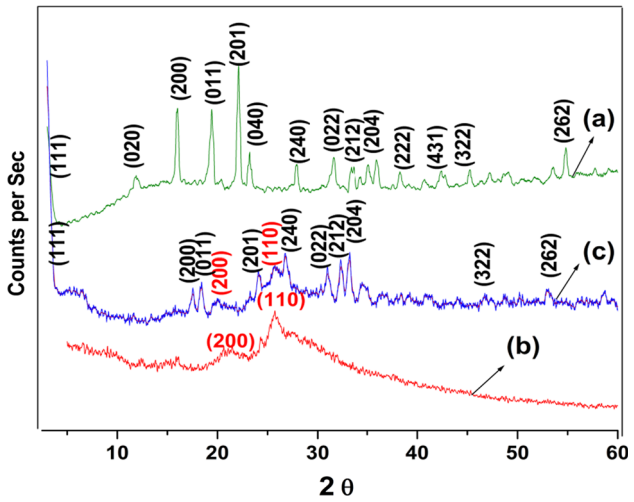

Figure 2 XRD of (*a*) SNP, (*b*) PANI and (*c*) PANI–NP composite.

polyaniline and polyaniline–nitroprusside composite. XRD of SNP shows sharp peaks at 2θ values of 3.27°, 12.03°, 16.69°, 19.50°, 22.26°, 23.23°, 28.10°, 31.83°, 33.61°, 35.72°, 38.31°, 42.53°, 45.29° and 54.86°. These peaks match well with the reported literature [24]. The peaks at angles of 2θ = 21.12° and 25.82° are attributed to the periodic repetition of benzenoid and quinoid rings in the PANI chains [27]. The peaks of PANI appear in the PANI–NP composite at 2θ values of 20.15° and 25.51°. In addition, the main reflections of SNP are observed in the PANI–NP composite at 2θ values of 3.44°, 17.55°, 18.36°, 24.20°, 26.96°, 31.01°, 32.47°, 33.29°, 46.75° and 52.92°. The peaks of SNP have shown a shift of ±1° in the PANI–NP composite, which indicates a successful interaction between the polyaniline and nitroprusside metal complex ion [28]. According to the XRD patterns of PANI–NP composite, it can be seen that almost all the diffraction peaks of nitroprusside are present, so the crystal structure of nitroprusside metal complex ion is retained during the polymerization of aniline. Moreover, the intensity of nitroprusside peaks in the PANI–NP composite is weaker and that may be due to the composition and amorphicity of PANI. Pure PANI is amorphous while the PANI–NP composite shows ordered structure, revealing the impact of nitroprusside metal complex ion on the polymer matrix.

FTIR characterization

FTIR of SNP, Pure PANI and PANI–NP composite is shown in Fig. 3. SNP shows prominent peaks at 2350, 2135, 1937 and 660 cm^{-1} which are due to stretching

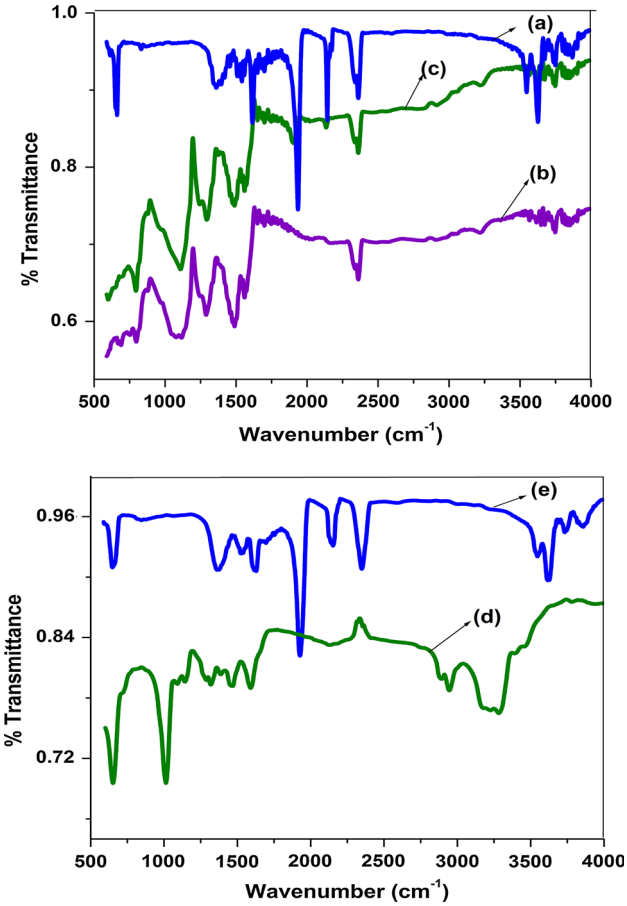

Figure 3 FTIR of (*a*) SNP (*b*) pure PANI (*c*) PANI–NP composite (*d*) PANI after MB adsorption and (*e*) PANI–NP composite after MB adsorption.

vibrations of –C≡N (axial and equatorial positions), –NO and Fe–C≡N, respectively [26]. These peaks appear in the PANI–NP composite at 2372, 2139, 1916 and 608 cm^{-1}, respectively. The FTIR spectra of pure PANI shows characteristic peaks at 3375, 1587, 1494, 1258, 1018 and 919 cm^{-1}. These peaks are due to N–H stretching vibration, C=C stretching vibration of quinoid and benzenoid segments of polyaniline, C–N stretching of the secondary aromatic amine, aromatic C–H in plane bending and an aromatic C–H out of plane bending vibration, respectively [29, 30]. The FTIR peaks of PANI appear in the composite at 3214, 1580, 1489, 1298, 1076 and 804 cm^{-1}, respectively. The shift of wavenumbers from pure PANI to PANI composite is because of the impact of nitroprusside metal complex on the PANI matrix.

FTIR is a useful tool that gives information about the possible interactions between the dye molecules and the adsorbent. FTIR spectra of PANI and PANI–NP composite after adsorption are shown in Fig. 3d,

e. FTIR of pure PANI and PANI–NP composite was compared before and after the adsorption of MB. There is a significant shift of wavenumbers in the FTIR of PANI before and after adsorption. The peak in the FTIR of PANI after MB adsorption at 3580 cm^{-1} indicates that water has been absorbed by the PANI during the adsorption. The shift of wavenumbers observed in the FTIR of PANI before and after MB adsorption is attributed to the strong interaction between MB dye molecules and the PANI adsorbent [16]. These results suggest the chemisorption type of interaction between the adsorbate and adsorbent. In the FTIR spectrum of PANI–NP composite, peaks at 2355, 2138, 1940 and 665 cm^{-1} are due to stretching vibrations of –C≡N (axial and equatorial positions), –NO and Fe–C≡N, respectively [26]. These characteristic peaks of nitroprusside appear in the FTIR of PANI–NP composite after adsorption at wavenumbers of 2355, 2139, 1916 and 608 cm^{-1}, respectively. As can be seen from the FTIR spectra of PANI–NP composite before and after adsorption, a significant shift of wavenumbers occur from 3310, 1618, 1528 and 1369 to 3240, 1582, 1486 and 1305 cm^{-1}, respectively. This further confirmed the interaction between the MB dye molecules and the PANI–NP composite. These are the characteristic peaks of polyaniline and are due to N–H stretching vibration, C=C stretching vibrations, C–N stretching vibration and C–H out of plane and bending vibrations, respectively. The shift of wavenumbers suggests chemical adsorption type of bonding between MB and PANI–NP composite. The FTIR peaks are very intense in pure PANI and PANI–NP composite before adsorption and shows widening after adsorption. The peak widening can be attributed to the impact of adsorbate molecules on the conjugated electronic structure of polymer backbone.

Thermogravimetric (TG) analysis

TG-DTG curve of PANI and composite of PANI with nitroprusside complex are shown in Fig. 4a, b. PANI shows two transitions. The first one is due to loss of water molecules that must be embedded in its outer layers and low molecular weight of polyaniline molecules, occurs in the temperatures range of 131–218 °C with a weight loss of 39%. The DTG maximum temperature corresponding to this transition is 195 °C. The second transition is observed in the temperature range of 218–730 °C with a weight loss of 47%, which can be due to decomposition of polyaniline chain. The DTG maximum temperature of this transition is 321 °C.

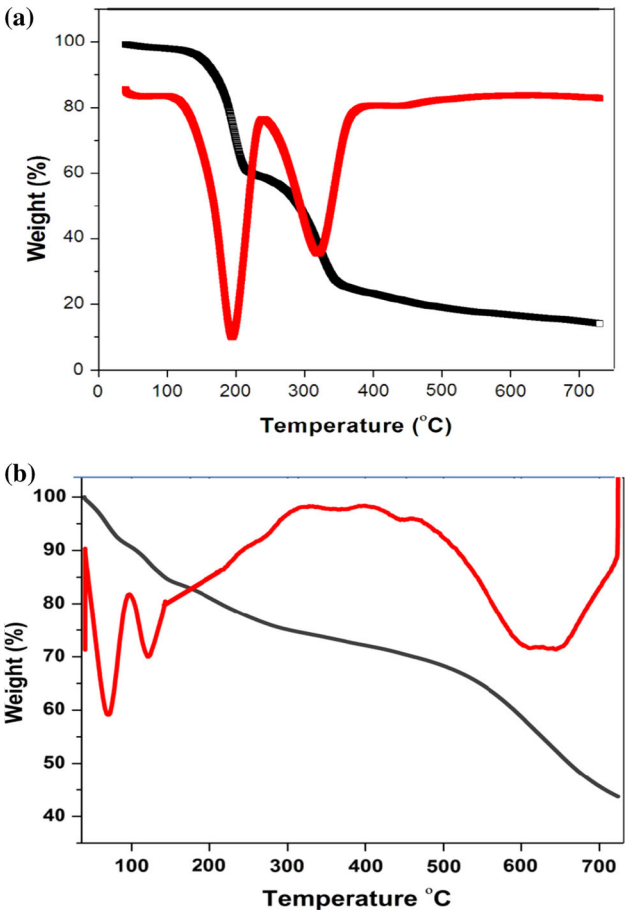

Figure 4 TG-DTG of **a** PANI and **b** PANI–NP composite.

The composite of PANI shows three transitions. The first one starts from 55 °C and ends at 119 °C with a weight loss of 7% which may be because of (1) loss of water molecules that might have been embedded in its outer layers and (2) loss of water of crystallization of dopant. The DTG maximum temperature of this transition is 69 °C. The second transition occurs at about 119 °C and ends at 298 °C with a weight loss of 13%. The DTG maximum temperature corresponding to this transition is 130 °C. The second transition is attributed to the loss of low molecular weight polyaniline. The third transition occurring in the temperature range of 298–730 °C with maximum DTG temperature of 615 °C can be ascribed to the decomposition of polyaniline chains and breakdown of organic part of dopant. This step accounts for 37.36% weight loss.

T_i (T_i is the temperature at which the transition occurs) is the parameter that compares the thermal stability of molecules. Higher value of Ti indicates a higher thermal stability [26]. T_i of pure PANI and PANI composite is 218 and 298 °C respectively. From this result it is clear that there has been an increase in the value of T_i in case of composite when compared with pure polyaniline, hence the composite material proves to have better thermodynamic stability than pure polyaniline.

On comparing the thermograms of polyaniline and composite, polyaniline shows 86% degradation at 730 °C and the composite shows the total weight loss of 57.36% up to 730 °C. This data suggests that the composite is thermally more stable than pure PANI. The reason is because of the strong electrostatic force of attraction between protonic amine groups of polyaniline and metal complex ion of nitroprusside (NH^+–$[Fe(CN)_5NO]^{2-}$). A strong electrostatic force of attraction between the components restricts the thermal motion of polyaniline in the composite and hence enhances the thermal stability of composite.

UV–visible spectral characterization

The UV–Vis spectra of PANI and PANI composite are shown in Fig. 5a. A UV–Vis spectrum of PANI shows two peaks at 313 nm and 462 nm. These peaks are due to π–π^* and n–π^* transition of benzenoid and quinoid segments of PANI, respectively. The UV–Vis spectrum of PANI–NP composite shows two peaks at 317 nm and 475 nm which are due to π–π^* and n–π^* transition of benzenoid and quinoid segments of PANI, respectively. Comparing the spectra of PANI and PANI–NP composite, a red shift has been observed that can be attributed due to the polaronic and bipolaronic formation in the PANI matrix due to the insertion of nitroprusside metal complex [31].

Energy band gap of PANI and PANI–NP composite is determined from absorption spectra using Tauc's relation by using Eq. 2.

$$\alpha h\nu = A\left[h\nu - E_g\right]^n \quad (2)$$

where $h\nu$ is energy of photon, h is Planck's constant, α is absorption coefficient, A is the constant and E_g is the optical energy band gap and n is the index describing electron transition. n has discrete values 0.5, 1.5, 2 and 2.5 for direct allowed, direct forbidden, indirect allowed and indirect forbidden transitions, respectively. From the plot of $(\alpha h\nu)^n$ versus $h\nu$, linear

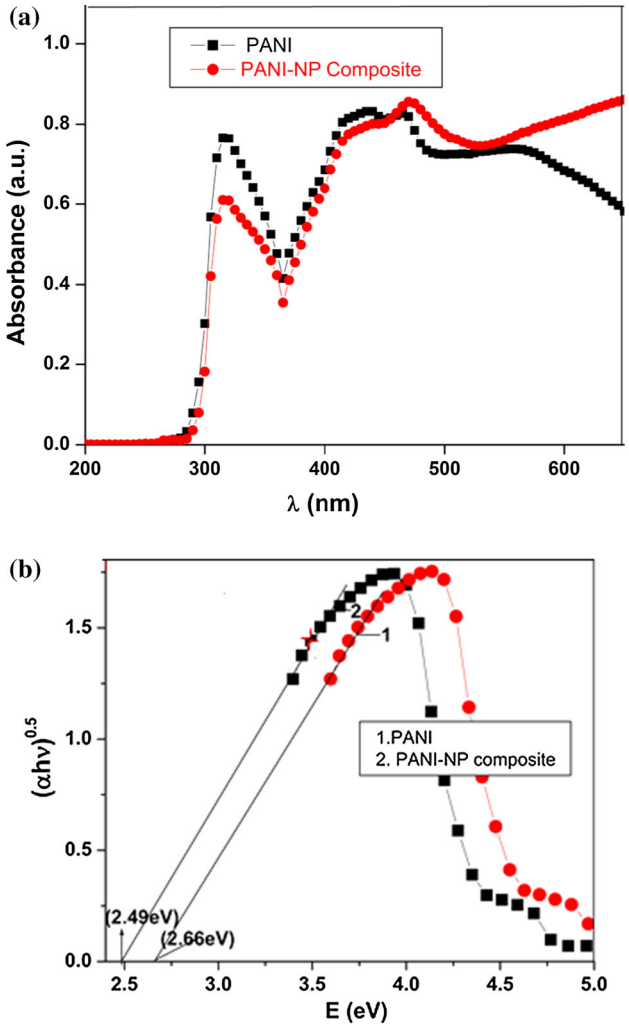

Figure 5 **a** UV–Vis spectra of PANI and PANI–NP composite and **b** band gap determination of PANI and PANI–NP composite using Tauc's relation.

fit is observed for $n = 0.5$, for both PANI and PANI–NP composite indicating the transition to be direct allowed transition as shown in Fig. 5b. By extrapolating $(\alpha h\nu)^{0.5} = 0$, band gap obtained for PANI and PANI–NP composite is found to be 2.66 and 2.49 eV, respectively. This decrease in band gap is ascribed to the perturbation of energy levels due to the influence of metal complex.

Transmission electron microscope (TEM) characterization

TEM images of PANI and PANI–NP composite are shown in Fig. 6a, b, respectively. TEM of pure PANI shows a network of interconnected PANI chains while TEM of PANI–NP composite shows a two

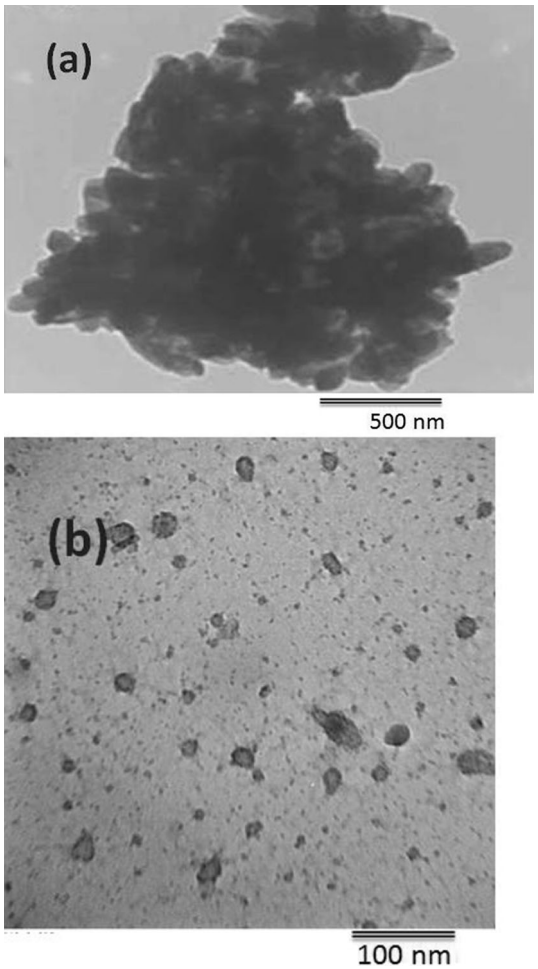

Figure 6 TEM images of **a** PANI and **b** PANI–NP composite.

phase system with nitroprusside particles embedded in the PANI matrix scattered randomly. The average particle size of nitroprusside particles is found to be 22 nm as calculated from TEM image of PANI–NP composite. Some nitroprusside particles are big suggesting the agglomeration of particles. Comparative analyses of both images confirm successful composite formation. Small particles have large surface area. The large specific surface area of PANI–NP composite is also confirmed from adsorption experiments via Brunaur–Emmet–Teller (BET) method. The larger the specific surface area, the greater would be its adsorption capacity.

Field emission scanning electron microscope (FESEM) characterization

FESEM pictures of PANI–NP composite before and after adsorption are shown in Fig. 7a, b, respectively.

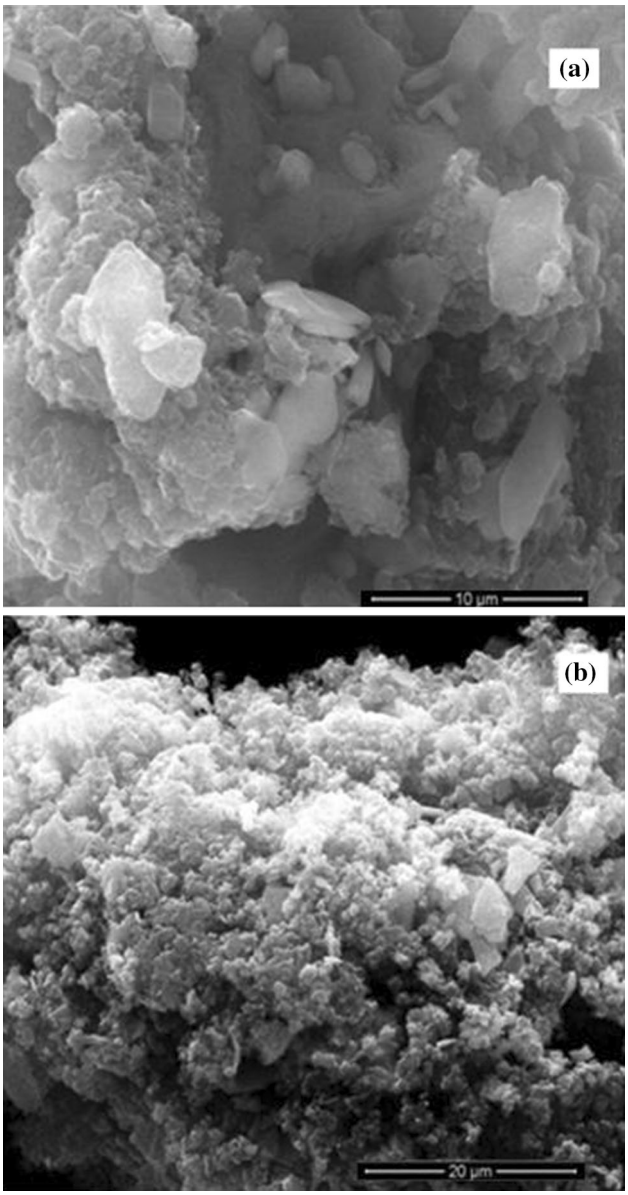

Figure 7 FESEM pictures of PANI–NP composite **a** before and **b** after MB adsorption.

Figure 7 shows plate like structures that confirm the presence of nitroprusside crystals embedded in the PANI matrix. Moreover the spongy mass and visible groves in Fig. 7a, is because of the amorphicity of PANI component. FESEM of PANI–NP composite as shown in Fig. 7b shows agglomeration of MB molecules, the size of which are in micrometers rather than existing as separate molecules. Due to the MB coverage on the PANI–NP composite, groves and plate like structures almost disappear, thus confirming the successful adsorption of MB onto PANI–NP composite.

Effect of contact time

Time-resolved absorption spectra of Methylene blue adsorption by polyaniline and polyaniline–nitroprusside composite are shown in Fig. 8. Absorbance of MB solutions is measured by UV–visible spectrophotometer. MB in aqueous solution shows maximum absorbance at 655 nm. It has been observed that the concentration of MB continuously decrease on increasing the contact time with the adsorbent. A fall in the concentration of MB in aqueous solution was observed as a result of the adsorption by polyaniline and polyaniline–nitroprusside composite. The shift of λ_{max} of MB occurs after the addition of adsorbent from 665 to 663 nm as a result of the interactions between MB dye molecule and PANI backbone. Polyaniline–nitroprusside composite is found to be far better adsorbent than PANI, taking the synergic benefits of both nitroprusside complex ion and polyaniline. Efficient and instantaneous adsorption of MB to the extent of 99.37% within 5 min duration occurs at room temperature, shows the ability of the material for many industrial applications. A scheme showing the adsorption of MB by pure PANI and PANI–NP composite is shown in Fig. 9.

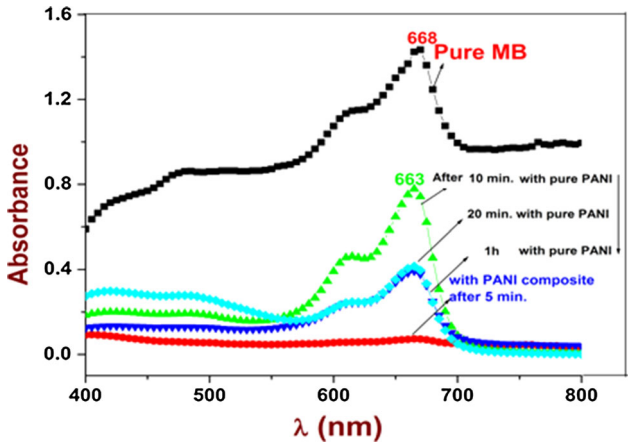

Figure 8 Time-resolved absorption spectra of MB aqueous solution.

Effect of adsorbent dosage

To investigate the effect of adsorbent dosage on the adsorption of MB, a series of experiments are carried out with the fixed quantity of MB solution (50 mL of 50 mg L^{-1} MB) as a test probe. As can be seen from the Table 1, removal percentage of MB from aqueous solution increases with the increase in the amount of adsorbent. However the increase is much higher for polyaniline–nitroprusside composite as compared to PANI. The reasons can be attributed to the large specific surface area of composite and negative charge density of nitroprusside complex ion $[Fe(CN)_5NO]^{2-}$. Nitroprusside being negatively charged can adsorb positively charged MB through electrostatic interaction. Of the two adsorbents used in the study, polyaniline–nitroprusside composite shows greater removal at all levels of the adsorbent dose than pure PANI.

Table 1 Effect of adsorbent dosage on the removal percentage of MB from aqueous solution

Dosage (*g*)	0.2	0.3	0.4	0.5
PANI	66.06	72.14	78.34	85.41
PANI–NP composite	86.45	92.87	96.46	99.37

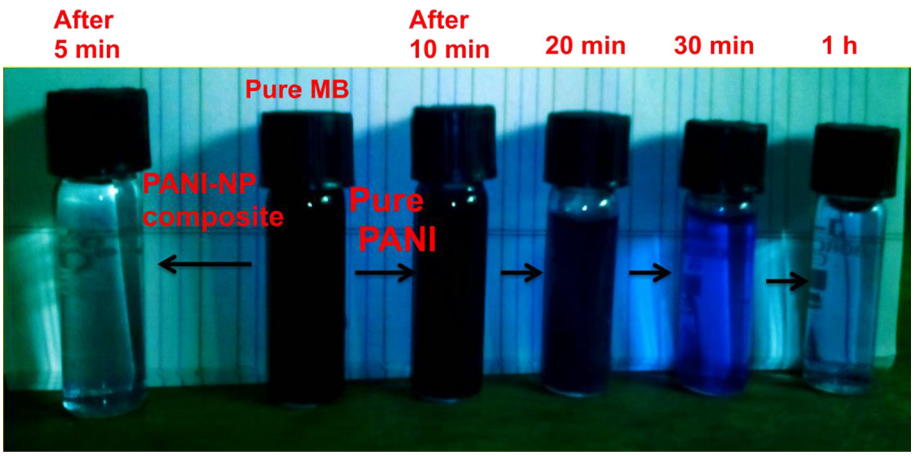

Figure 9 Images of MB aqueous solution before and after treated with PANI and PANI–NP composite.

Efficiency removal

The percentage removal of MB from aqueous solution is calculated using the following equation:

$$\eta = \frac{C_i - C_t}{C_i} \times 100 \quad (3)$$

where C_i is the initial concentration of MB and C_t is the concentration at time 't' in mg L^{-1}.

The maximum amount of MB adsorption at equilibrium is determined using the following equation:

$$Q_e = \left(\frac{C_i - C_e}{C_i}\right)\frac{V}{M} \quad (4)$$

where V is the volume of solution and M is the mass of adsorbent.

The adsorption of MB is investigated in the range of 10–60 min in case of PANI and 2–5 min for polyaniline–nitroprusside composite as summarized in Table 2. With MB, PANI exhibits maximum adsorption capacity in 1 h while as PANI–NP composite exhibits a highly improved and efficient adsorption to the extent of 99.37% in just 5 min. The measured adsorption capacities are 412.80 and 496.85 mg g^{-1}, for polyaniline and polyaniline–nitroprusside composite.

The efficiency of removal of PANI–NP composite is much higher than polyaniline probably because of high charge density of nitroprusside metal complex ion and large specific surface area. The maximum adsorption capacities for MB by polyaniline and polyaniline–nitroprusside composite are higher than reported data as shown in Table 3 [2, 23, 32–38]. Polyaniline containing nitrogen atoms with lone pair of electrons can pick up MB dye molecules from the solution through electrostatic interaction. Further the π-electrons of benzenoid and quinoid segments of polyaniline can interact with the π-electrons of MB through π–π coupling [36]. There are C=C double bonds in the MB molecule. The mechanism of adsorption of MB on polyaniline–nitroprusside composite is a complex one, involving more than one type of interactions. Electrostatic attraction between

Table 2 Efficiency removal and maximum adsorption capacities of polyaniline and polyaniline–nitroprusside composite towards MB

Time (min)	Efficiency removal (%) PANI	Maximum adsorption capacity (mg g^{-1}) PANI	Time (min)	Efficiency removal (%) PANI–NP composite	Maximum adsorption capacity (mg g^{-1}) PANI–NP composite
0	0	0	0	0	–
10	55.78	350.12	1	86.88	444.08
20	72.32	379.15	2	90.12	450.05
30	78.10	388.08	3	92.56	460.5
40	84.32	398.53	4	94.68	473.25
60	85.41	412.80 (Q_e)	5	99.37	496.85 (Q_e)

Table 3 Maximum adsorption capabilities for MB by different adsorbents

Adsorbents	Adsorption capability (mg g^{-1})	C_0 (mg L^{-1})	References
Polypyrrole/sawdust composite	34.36	50	[2]
Palygorskite	158.03	100	[33]
Pinecone biomass	109.89	40 (PP mL^{-1})	[32]
nMn-bamboo composite	322.50	140	[34]
Graphene–polypyrrole composite	270.3	100	[35]
Polyacrylic acid/$MnFe_2O_4$ composite	53.3	8.3	[36]
Chitosan-*g*-polyacrylic acid montmorillonite composite	185.9	200	[23]
Epichlorohydrin alginate beads	229.18	100	[38]
Magnetite porous carbons	305.95	50	[37]
PANI (emeraldine base)	412.80	50.5	Present work
PANI–NP composite	496.85	50.5	Present work

oppositely charged sites plays a dominant rule in the adsorption of MB. Nitroprusside being negatively charged makes the surface of polyaniline–nitroprusside composite an anionic polymer. This property makes it a suitable adsorbent for cationic dyes like MB. The proposed mechanism for the adsorption of MB dye onto pure PANI and PANI–NP composite is shown in Scheme 1. The specific surface area is one of the important factors that determine the adsorption affinity of an adsorbent. As shown in Table 4, the specific surface area of polyaniline–nitroprusside composite is much higher than pure PANI. This describes and justifies the role of metal complex in the polyaniline–nitroprusside composite in improving its surface area. Large surface area of polyaniline–nitroprusside composite means an increase in the exposure of active adsorption sites of composite. These results suggest that the polyaniline–nitroprusside composite is the best adsorbent than any other adsorbent reported in the literature for the removal of MB in terms of its high efficiency (99.37%) and greater value of adsorption capability (496.86 mg g^{-1}).

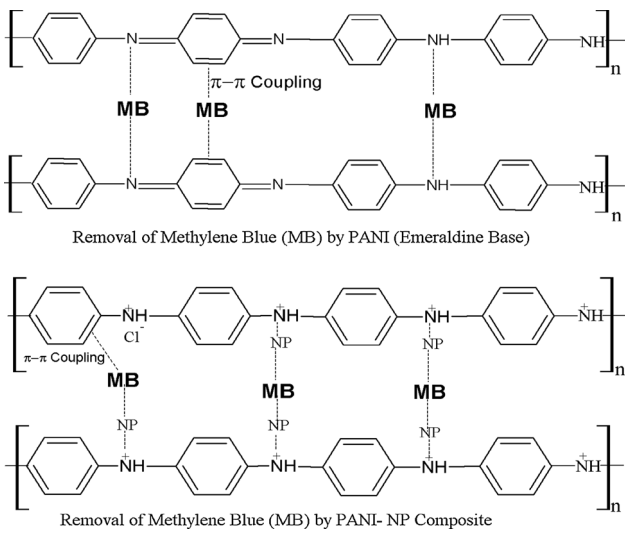

Scheme 1 Proposed mechanism for the adsorption of MB dye by PANI and PANI–NP composite.

Effect of initial concentration of MB dye

More than 99% of the adsorption of MB onto PANI–NP composite occurs within 5 min. This can be because of the electrostatic attraction between the cationic MB dye molecule and negatively charged surface of polyaniline–nitroprusside composite. The adsorption slightly decreases with the increase in the concentration of MB, as a result of the saturation of the adsorption sites and due to the aggregation of MB dye molecules. This makes it impossible for MB molecules to diffuse deeper into the porous structure of polyaniline–nitroprusside composite.

As shown in Table 5, the adsorption capacity of polyaniline–nitroprusside composite is much higher than that of pure PANI under the same initial dye concentration. This can be due to the large specific surface area and negatively charged surface of polyaniline–nitroprusside composite.

Effect of pH

The adsorption of MB onto the pure PANI and PANI–NP composite depends on the pH of the solution. Pure PANI shows good adsorption in alkaline medium and less in acidic solution. At low pH (2), PANI chains are highly protonated, thus, develops a positive charge throughout the adsorbent, therefore, shows low adsorption affinity towards MB elimination from the conc. HCl solution. At higher pH (10), protonic imine groups would be deprotonated leaving behind the nitrogens with lone pairs, as a result it can exert attractive force on the cationic MB dye molecule. Thus, in conc. NaOH solution, PANI shows excellent adsorption for MB. However the adsorption of MB onto polyaniline–nitroprusside composite is totally reversed to what has been observed with pure PANI in acidic and alkaline environment. It shows good adsorption in acidic solution (pH 2), due to the observation that nitroprusside metal complex ion $[Fe(CN)_5NO]^{2-}$ in the composite, due to electrostatic attraction adsorbs cationic MB and simultaneously neutralizes the effect

Table 4 The specific surface area and removal rate of PANI and PANI–NP composite for MB

Sample	Specific surface area (m^2 g^{-1})	Removal efficiency (%)
Sodium nitroprusside (SNP)	28	
PANI	4	78.67
PANI–NP composite	30	99.37

Table 5 Effect of initial concentration (C_0) of MB on the adsorption by PANI and polyaniline–nitroprusside composite

C_0 (mg L^{-1})	50	60	70	80
Adsorbent	Adsorption %			
PANI	85.41	79.32	77.86	72.42
PANI–NP composite	99.37	99.31	95.35	92.22

Table 6 Effects of solution pH on adsorption percentage of MB onto PANI and PANI–NP composite

pH	2	4	8	10
PANI (EB)	65.13	75.24	86.05	86.35
PANI–NP composite	99.43	99.39	96.32	95.11

of excess of H^+ ions in the solution. In basic solution (pH 8), adsorption affinity of PANI–NP composite is low owing to the electrostatic repulsion between the hydroxyl group and nitroprusside metal complex ion of the composite. The hydroxyl ions present in the solution neutralizes the charge of MB as a result it retards the adsorption affinity of PANI–NP composite for MB. The results obtained are provided in Table 6. Change of pH solution has caused a significant change in the adsorption percentage of MB onto PANI but a little effect has been observed in case of PANI–NP composite.

Adsorption kinetics

The pseudo-first order, pseudo-second order and intraparticle diffusion models are used to evaluate the kinetic mechanism, which controls the adsorption process. Validity of the models are verified by the linear equation analysis log $Q_e - Q_t$ versus t, t/Q_t versus t and Q_t versus $t^{1/2}$, respectively.

The adsorption of liquid–solid systems based on solid capacity is well described by Lagergren kinetic equation. This equation is based on the concentration of the solution and adsorption capacity of the solid [39]. Lagergren first order rate equation is called pseudo-first-order reaction. The first model is the pseudo- first order equation shown in Eq. 5.

$$\text{Log}\,(Q_e - Q_t) = \log Q_e - \frac{k_1}{2.303}\,t \tag{5}$$

where Q_e and Q_t (mg g^{-1}) refer to the amount of MB adsorbed at equilibrium and time t (min), respectively, and k_1 is the rate constant.

The pseudo-second-order rate expression is based on the adsorption capacity of solids but contrary to the first model it describes chemisorptions over the whole adsorption time [39]. The pseudo-second order model equation is represented by Eq. 6.

$$\frac{t}{Q_t} = \frac{1}{k_2 Q_e^2} + \frac{t}{Q_e} \tag{6}$$

where k_2 is the rate constant of the pseudo-second order model.

The initial adsorption rate "h" [mg (g min)$^{-1}$] is calculated from k_2 and Q_e by the Eq. 7.

$$h = k_2 Q_e^2 \tag{7}$$

The intra-particle diffusion model of Weber and Morris is represented by the Eq. 8.

$$Q_t = k_i t^{1/2} + C \tag{8}$$

where k_i is an intraparticle diffusion rate constant and C is the concentration of adsorbate (mg L^{-1}).

Figures 10, 11 and 12, shows fitting plots for pseudo-first order, pseudo-second order and intraparticle diffusion models, respectively. The kinetic parameters (rate constants and correlation coefficients) obtained from fitting results are presented in Table 7. On the basis of the value of correlation coefficients (R^2), the pseudo-first order is the best model to describe the adsorption of MB onto polyaniline and pseudo-second order for the PANI–NP composite. However the concordance in the experimental and calculated Q_e values, also suggests the adsorption of MB onto PANI–NP composite via pseudo-second order kinetics. Thus, pseudo-second order reaction can be applied to investigate the kinetics of MB adsorption onto PANI–NP composite. Initial adsorption rate is very high for both PANI and PANI–NP composite. The value of 'h' in case of PANI–NP composite is about 2.2 times that of pure PANI is due to the effect of nitroprusside metal

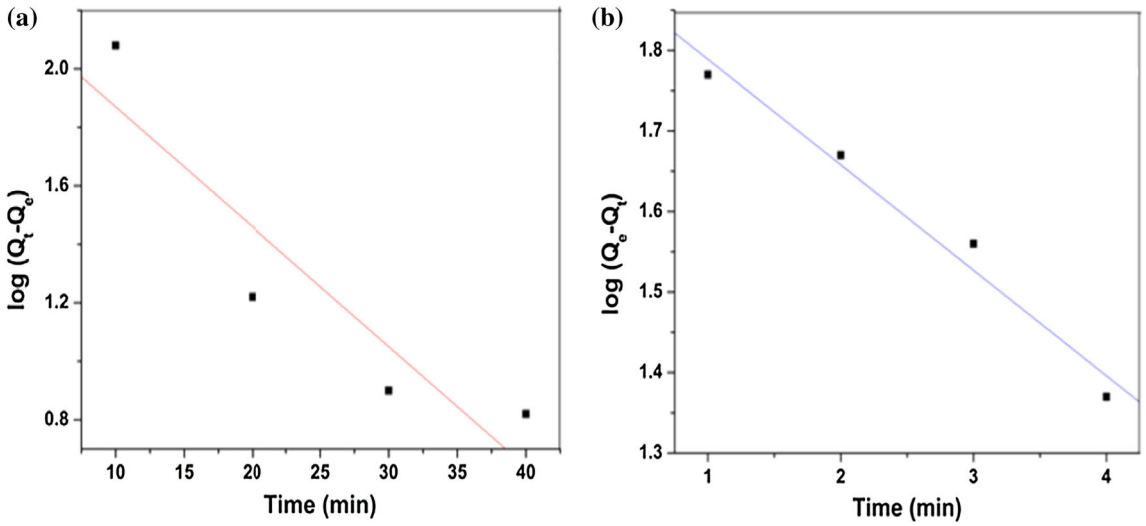

Figure 10 Pseudo-first order plot for MB adsorption by **a** PANI and **b** PANI–NP composite.

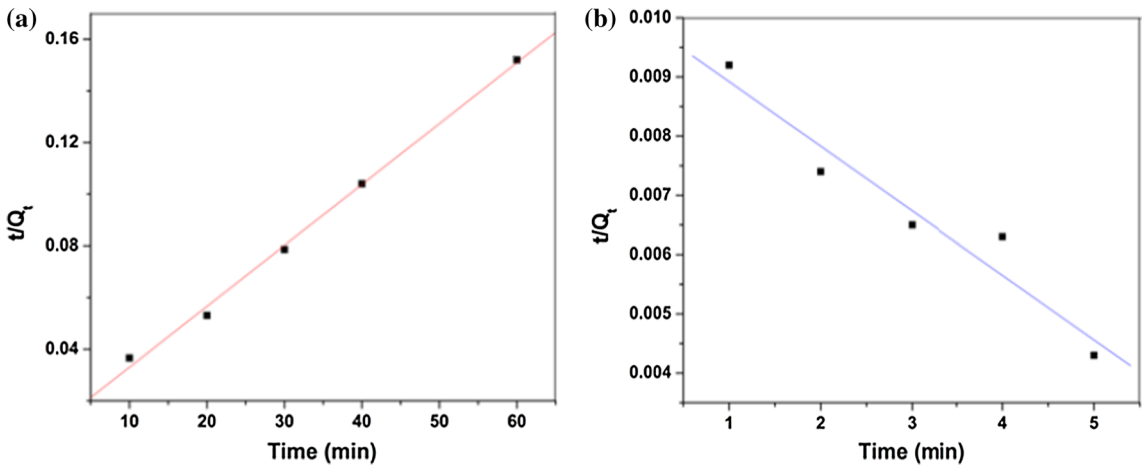

Figure 11 Pseudo-second order plot for MB adsorption by **a** PANI and **b** PANI–NP composite.

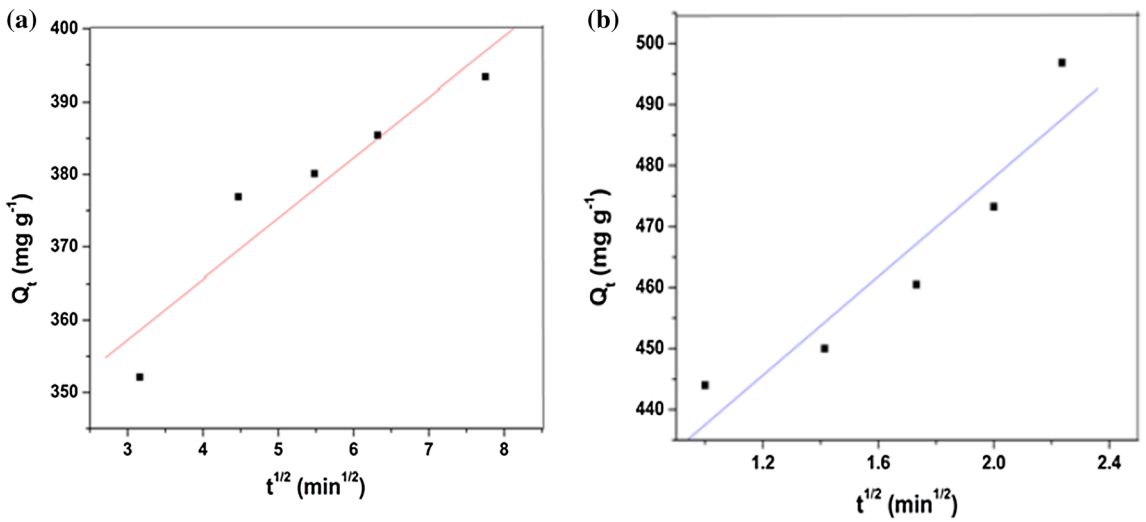

Figure 12 Intraparticle diffusion plot for MB adsorption by **a** PANI and **b** PANI–NP composite.

Table 7 Kinetic parameters for MB adsorption by polyaniline composite

Composite materials	Type	Parameters			
	Pseudo-first order kinetics	k_1 (min^{-1})	Q_e (mg g^{-1})	R^2	
PANI		0.133	371.24	0.98835	
PANI–NP composite		0.179	398.28	0.91830	
	Pseudo-second order kinetics	k_2 (min^{-1})	Q_e (mg g^{-1})	R^2	h [mg (g min)$^{-1}$]
PANI		0.143	372.41	0.93910	1.98×10^4
PANI–NP composite		0.182	489.75	0.99228	4.36×10^4
	Intra-particle diffusion model	k_i [g (mg min^{-1})]	C_e (mg L^{-1})	R^2	
PANI		2.547	41.64	0.93916	
PANI–NP composite		4.310	51.58	0.97354	

complex ion in the composite. Electrostatic force of attraction between nitroprusside and MB could be one of the reasons of increase of adsorption of MB onto PANI–NP composite. Large surface area of composite also favours the adsorption of MB onto the composite.

Adsorption isotherm

The following adsorption isotherms are used to fit the experimental data: (1) Langmuir model (2) Freundlich model and (3) Tempkin model.

Langmuir model is expressed by Eq. 9.

$$\frac{C_e}{Q_e} = \frac{1}{K_L Q_{max}} + \frac{C_e}{Q_{max}} \tag{9}$$

where C_e, is the equilibrium concentration of the adsorbate and Q_{max} is the adsorption capacity at saturation (mg g^{-1}). K_L is the Langmuir adsorption constant and is related to the energy of adsorption.

A dimensional factor called separation factor 'R_L' is an essential feature of the Langmuir isotherm and is defined by Eq. 10.

$$R_L = \frac{1}{(1 + K_L C_i)} \tag{10}$$

where C_i (mg L^{-1}), is the initial MB concentration. The value of R_L indicates the shape of the isotherm. Adsorption is unfavourable if $R_L > 1$, linear ($R_L = 1$) and favourable if $0 < R_L < 1$ or even reversible if $R_L = 0$ [40].

Freundlich model is expressed by Eq. 11.

$$\ln Q_e = \ln K_F + \frac{1}{n} \ln C_e \tag{11}$$

where n is the Freundlich constant, K_F is the other constant related to the maximum adsorption capacity.

Tempkin model is represented by Eq. 12.

$$Q_e = B \ln K_T + B \ln C_e \tag{12}$$

where K_T is the equilibrium binding energy constant and B is a constant related to the energy of adsorption. Tempkin Isotherm is based on two assumptions [41]. Ist assumption is related with the enthalpy of adsorption and states that ΔH_{ads}. of all the adsorbated molecules in the layer decreases linearly with coverage. Second assumption assumes that the adsorption process depends on the density and distribution of functional groups present on the dye and adsorbent surface.

Figures 13, 14 and 15, show the linearalized Langmuir, Freundlich and Tempkin plots of MB adsorption by polyaniline and PANI–NP composite, respectively. The adsorption isotherm parameters calculated from the slope and intercept of the linear equations are shown in Table 8. Investigation of isothermal characteristics revealed that adsorption of MB onto PANI and PANI–NP composite are in high agreement with the Langmuir model. The value of R^2 is maximum for both PANI and PANI–NP composite indicates a Langmuir type of adsorption. This suggests monolayer coverage of MB and a chemisorptions type of bonding between the adsorbate and adsorbent. There are two types of chemisorption: associative chemical adsorption and dissociative chemical adsorption. From experimental data and observation, it appears, that associative chemical

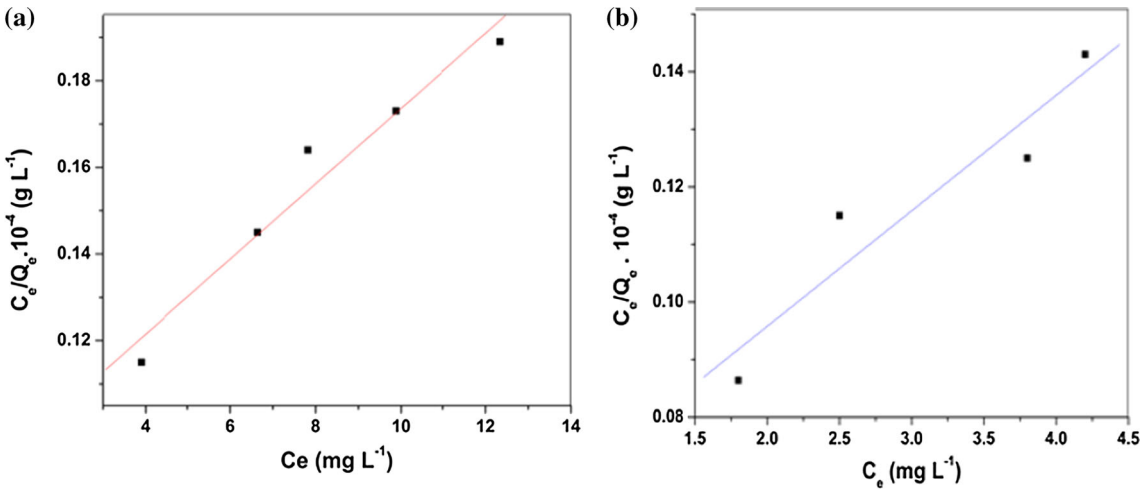

Figure 13 Langmuir isotherm plot for MB adsorption by **a** PANI and **b** PANI–NP composite.

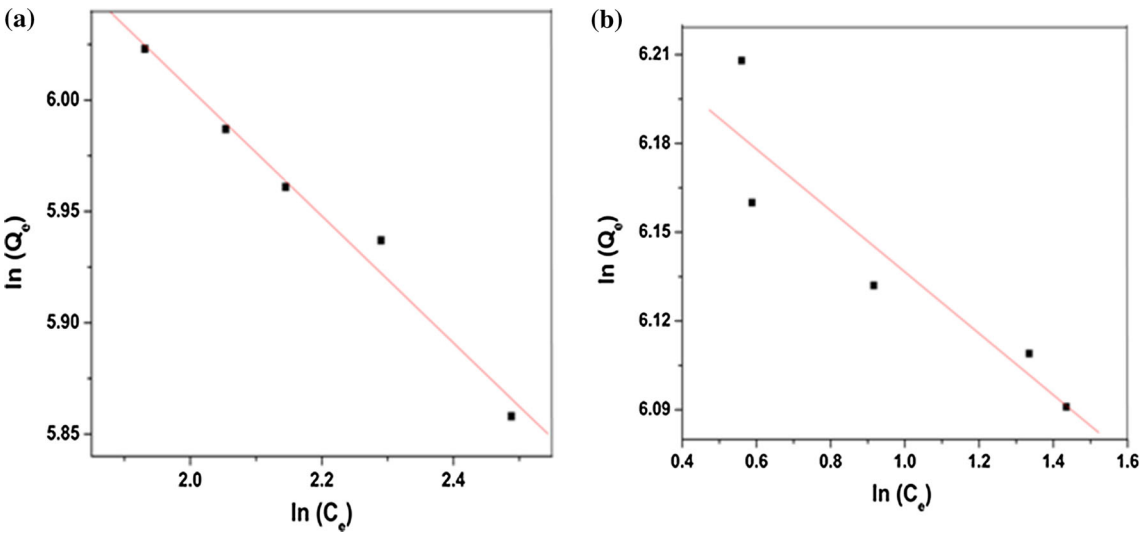

Figure 14 Freundlich isotherm plot for MB adsorption by **a** PANI and **b** PANI–NP composite.

adsorption occurs between MB and PANI backbone. Due to the chances of π–π coupling between π-electrons of MB and PANI alters the electronic structures which can induce the adsorption capacity in the composite material. Strength of bonds in associative chemical adsorption changes but not dissociates. Large value of '*B*' as calculated in Tempkin model for both PANI and PANI–NP composite also suggests the chemical adsorption type of bonding between adsorbate and adsorbent, thus, it agrees with the Langmuir model [42]. The value of K_L is related to the energy of adsorption [43]. The value of K_L is higher for PANI–NP composite than PANI suggests that the adsorption of MB onto composite is better described by Langmuir model than the adsorption onto pure PANI. The value of R_L has been found in the range of 0–1, indicating that the adsorption of MB onto PANI and PANI–NP composite through Langmuir model is favourable. R^2 value for both PANI and PANI–NP composite is more than 0.75 in Frendlich and Tempkin models, therefore, adsorption of MB is not limited to just a monolayer coverage. The value of n is greater than 1 in both cases, which suggests that the adsorption of MB through physiosorption is also possible. Physical nature of force between MB and adsorbents (PANI and PANI–NP composite) is also supported by thermodynamic study. Therefore, adsorption mechanism between MB and PANI backbone is a complex one, involving both types of adsorptions (physiosorption and chemisorption).

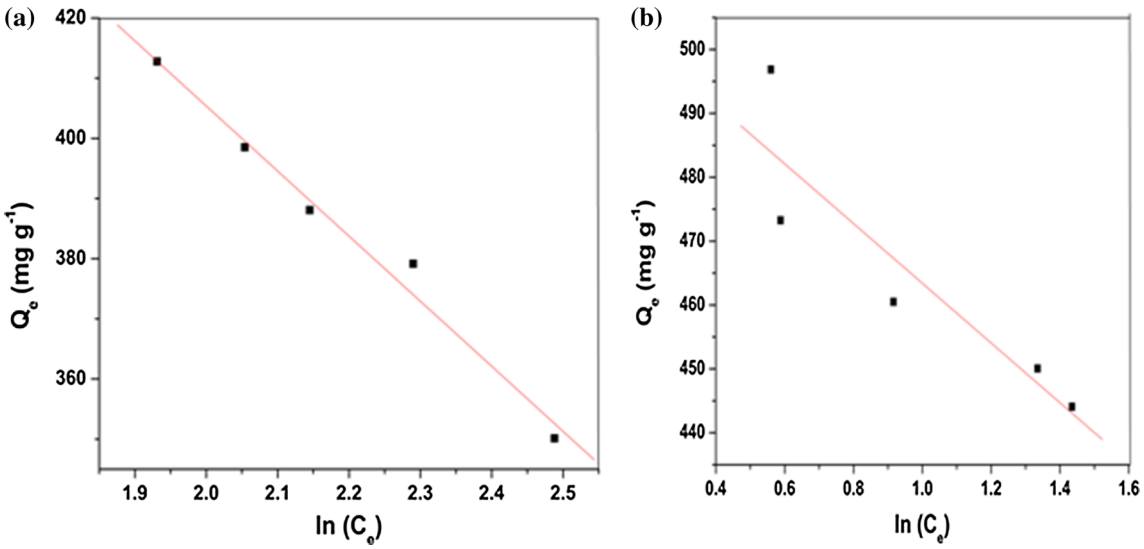

Figure 15 Tempkin isotherm plot for MB adsorption by **a** PANI and **b** PANI–NP composite.

Table 8 Parameter values of different adsorption models (calculated after linear fit method)

Composite materials	Model	Parameters		
	Langmuir	K_L (L g^{-1})	R_L	R^2
PANI		3.12	0.692	0.9477
PANI–NP composite		8.92	0.865	0.9984
	Freundlich	K_F (L g^{-1})	n	R^2
PANI		444.25	2.68	0.857
PANI–NP composite		66.40	1.80	0.789
	Tempkin	K_T (L mg^{-1})	B	R^2
PANI		1.86	23.54	0.8842
PANI–NP composite		3.25×10^{13}	112.44	0.8002

Thermodynamic study

Thermodynamic parameters (shown in Table 9) like change in entropy ($\Delta S°$), enthalpy change ($\Delta H°$) and standard Gibbs free energy change ($\Delta G°$) for the adsorption of MB from the aqueous solution onto PANI and PANI–NP composite are determined using Eqs. 13 and 14.

$$\ln (Q_e/C_e) = \frac{\Delta S^\circ}{R} + -\Delta H^\circ/RT \quad (13)$$

where Q_e is the amount of MB adsorbed per unit mass of adsorbent (mg g^{-1}), R is gas constant (J K^{-1} mol^{-1}) and T is the temperature. The ratio of ln (Q_e/C_e) is referred to as adsorption affinity. A plot of ln (Q_e/C_e) versus $1/T$ as shown in Fig. 16, gives the values of $\Delta S°$ and $\Delta H°$ from the intercept and slope, respectively. $\Delta G°$ is calculated by Gibbs–Helmholtz equation through Eq. 14.

$$\Delta G^\circ = \Delta H^\circ - T\Delta S^\circ \quad (14)$$

Rehman et al. [44] described the criteria for physiosorption and chemisorption between adsorbate and adsorbent on the basis of enthalpy change ($\Delta H°$): 4–10 kJ mol^{-1} (physical adsorption), 2–40 kJ mol^{-1} (Hydrogen bonding forces) and >40 kJ mol^{-1} (chemical adsorption). The $\Delta H°$ value for adsorption of MB on PANI is −27 kJ mol^{-1} and in case of PANI–NP composite, it is −0.894 kJ mol^{-1}. These results suggest the interactions between MB and adsorbents (PANI and PANI–NP composite) are a physically controlled process. The change of standard free energy ($\Delta G°$) for physiosorption is in the range of −20 to 0 kJ mol^{-1} and for chemisorptions varies between −80 and −400 kJ mol^{-1} [45]. The $\Delta G°$ value for the MB adsorption onto PANI at different temperatures ranges from −16.327 to −17.930 kJ mol^{-1} and −0.387 to −0.46 kJ mol^{-1} in case of PANI–NP composite. These results correspond to a physical adsorption between adsorbate and adsorbent.

The negative value of enthalpy change shows exothermic nature of the adsorption process and the negative value of entropy change indicates a decrease in the disorderdness at the solid/liquid interface. This suggests a strong type of bonding between the adsorbate and adsorbent. The negative value of $\Delta G°$ for both PANI and PANI–NP composite implies a spontaneous nature of the adsorption process. The

Table 9 Themodynamic parameters for the removal of MB by PANI and PANI–NP composite

Adsorbent	$\Delta G°$ (J mol^{-1})						$\Delta H°$ (J mol^{-1})	$\Delta S°$ (J K^{-1} mol^{-1})
	25 °C	35 °C	45 °C	55 °C	65 °C	75 °C		
PANI	−17930	−17609	−17291	−16968	−16650	−16327	−27486	−32.067
PANI–NP composite	−460	−445	−431	−416	−402	−387	−894.24	−1.456

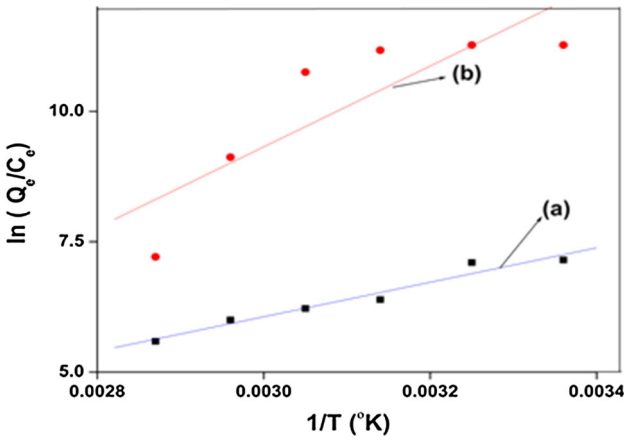

Figure 16 Plot to determine thermodynamic parameters of MB adsorption by *a* PANI and *b* PANI–NP composite.

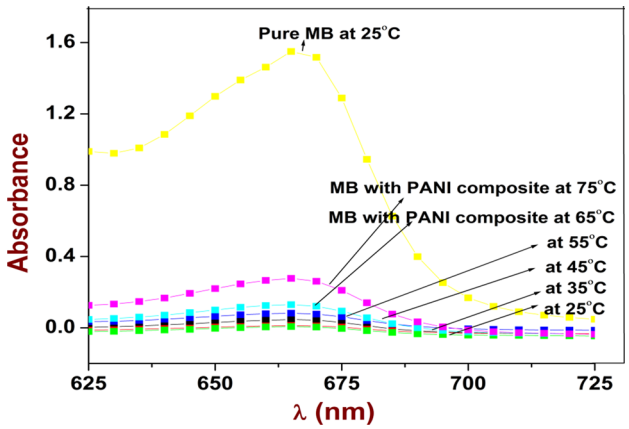

Figure 17 Visible spectra of MB aqueous solution treated with PANI–NP composite at different temperatures.

continuous decrease of $\Delta G°$ for both PANI and PANI–NP composite with the increase of temperature indicates that the adsorption process is turning into non-spontaneous one. It implies that at higher temperature, desorption occurs. Figure 17 shows the increase of desorption rate with the increase of temperature. Up to 55 °C, desorption occurs imperceptibly but after this temperature, the rate of desorption is found to increase significantly. Thus the data indicates that the PANI–NP composite is an efficient adsorbent in removing MB from aqueous solution up to 55 °C and beyond this temperature, the separation of MB from the adsorbent is possible. This increases the chances of adsorbent for reuse and regeneration. The results suggest that the PANI–NP composite is a potential candidate as efficient adsorbent towards MB removal from aqueous solution up to higher temperature (55 °C).

Desorption study

For the desorption study, 50 mg of MB is loaded on 0.5 g of PANI–NP composite by the adsorption procedure. Then, it is dissolved in 20 mL of water and the solution is stirred on magnetic stirrer for 5 min. Since adsorption of MB onto PANI–NP composite is an exothermic process, therefore, heating weakens the force of attraction between MB and PANI–NP composite and then MB desorption increases. Amount of desorbed MB in the eluting solution is determined spectrophotometrically, at 55°, 65° and 75 °C. The desorption percentage using Eq. 15 at 55°, 65° and 75 °C is calculated as 15.54, 18.65 and 25.24, respectively.

$$\text{Percentage desorption} = \frac{m_2}{m_i} \times 100 \tag{15}$$

where m_i is MB adsorbed in mg onto PANI–NP composite before elution and m_2 is the amount of MB desorbed in the eluting solution.

Since MB has been desorbed by water, it can be said that the bond between MB and PANI–NP composite is a weak one, suggesting the physiosorption type of bonding between the MB and adsorbent. In this way, desorption study helps in elucidating the adsorption mechanism between MB and PANI–NP composite.

Conclusion

Polyaniline and polyaniline–nitroprusside composite is synthesized via oxidative chemical polymerization method using ammonium persulphate as an oxidizing agent. UV–visible spectroscopy is employed to investigate the adsorption of MB onto pure PANI and PANI–NP composite. PANI–NP composite carries a

high density of localized negative charge, which makes it an ideal candidate for removal of cationic dye (MB) from aqueous solution. With the increase in specific surface area from pure PANI to PANI–NP composite, adsorption capacity has increased under the same initial concentration. Pure PANI shows good MB adsorption in alkaline solution whereas PANI–NP composite exhibits an efficient adsorption in acidic solution. From the kinetic data, pseudo-first order kinetics is followed for pure PANI and pseudo second order kinetics for PANI–NP composite. Langmuir Isotherm model is found to describe the equilibrium isotherm data for PANI as well as the PANI–NP composite. Thermodynamic parameters suggest the exothermic and spontaneous nature of the adsorption process. In FTIR, the shift of wavenumber of N–H stretching frequency in PANI and PANI–NP composite before and after adsorption shows the successful adsorption of MB molecules. Appearance of addition peak due to O–H stretching vibration of water in the FTIR of composite material shows the absorption of water during the adsorption of MB dye molecules. Peak broadening in the FTIR spectra of PANI and PANI–NP composite after adsorption further confirms the successful adsorption of MB. The adsorption efficiency and adsorption capacity values of PANI–NP composite are much higher than pure PANI which suggests that PANI–NP composite is far better adsorbent than pure PANI towards the removal of MB from aqueous solution. Thermogravimetric analysis confirms improved thermal stability of polyaniline composite upon doping with the metal complex (SNP).

Acknowledgements

We wish to express our gratitude to the research institutions of SAIF STIC Kochi and the Central Instrumentation facility, Jammia Millia Islamia, New Delhi, for providing the instrumentation facilities. The authors are also thankful to Prof. Rajat Gupta, Former Director of NIT Srinagar and Prof. Tabassum Ara, Head of the Department of Chemistry, NIT, for their support and cooperation.

References

[1] Ahmad A, Mohd-Setapar SH, Chuo SC, Khatoon A, Wani WA, Kumar R, Rafatullah M (2015) Recent advances in new generation dye removal technologies: novel search of approaches to reprocess waste water. RSC Adv 5:30801–30818

[2] Ansari R, Mosayebzadeh Z (2010) Removal of basic dye methylene blue from aqueous solutions using sawdust and sawdust coated with polypyrrole. J Iran Chem Soc 7(2):339–350

[3] Moussavi G, Mahmoudi M (2009) Removal of azo and anthraquinone reactive dyes from industrial wastewaters using MgO nanoparticles. J Hazard Mater 168:806–812

[4] Zendehdel M, Barati A, Alikhani H, Hekmat A (2010) Removal of methylene blue dye from wastewater by adsorption onto semi-inpenetrating polymer network hydrogels composed of acrylamide and acrylic acid copolymer and polyvinyl alcohol. Iran J Environ Health Sci Eng 7(5):423–428

[5] Zhang Y, Li Q, Sun L, Tang R, Zhai J (2010) High efficient removal of mercury from aqueous solution by polyaniline/humic acid nanocomposite. J Hazard Mater 175:404–409

[6] Gupta SS, Bhattacharyya KG (2012) Adsorption of heavy metals on kaolinite and montmorillonite: a review. Phys Chem Chem Phys 14:6698–6723

[7] Ogata F, Tominaga H, Kangawa M, Inoue K, Kawasaki N (2012) Adsorption capacity of Cu(II) and Pb(II) onto carbon fiber produced from wool. J Oleo Sci 61:149–154

[8] Hua M, Zhang S, Pan B, Zhang W, Lv L, Zhang Q (2012) Heavy metal removal from water/wastewater by nanosized metal oxides: a review. J Hazard Mater 211–212:317–331

[9] Qamar M, Gondal MA, Yamani ZH (2011) Laser-induced efficient reduction of Cr(VI) catalyzed by ZnO nanoparticles. J Hazard Mater 187:258–263

[10] Gupta SS, Bhattacharyya KG (2014) Adsorption of metal ions by clays and inorganic solids. RSC Adv 4:28537–28586

[11] Jiang Z, Xie J, Jiang D, Yan Z, Jing J, Liu D (2014) Enhanced adsorption of hydroxyl contained/anionic dyes on non functionalized Ni@SiO_2 core-shell nanoparticles: kinetic and thermodynamic profile. Appl Surf Sci 292:301–310

[12] Huang Y, Li J, Chen X, Wang X (2014) Applications of conjugated polymer based composites in wastewater purification. RSC Adv 4:62160–62169

[13] Samani MR, Borghei SM, Olad A, Chaichi MJ (2010) Removal of chromium from aqueous solution using polyaniline–poly ethylene glycol composite. J Hazard Mater 184:248–254

[14] Mahanta D, Madras G, Radhakrishnan S, Patil S (2008) Adsorption of sulfonated dyes by polyaniline emeraldine salt and its kinetics. J Phys Chem B 112:10153–10157

[15] Ai L, Jiang J, Zhang R (2010) Uniform polyaniline microspheres: a novel adsorbent for dye removal from aqueous solution. Synth Met 160:762–767

[16] Janaki V, Oh BT, Shanthi K, Lee KJ, Ramasamy AK, Kamala-Kanan S (2012) Polyaniline/chitosan composite: an eco-friendly polymer for enhanced removal of dyes from aqueous solution. Synth Met 162:974–980

[17] Ayad MM, Al-Nasr AB (2013) Anionic dye (acid green 25) adsorption from water by using polyaniline nanotubes salt/silica composite. J Nanostruct Chem 3:1–9

[18] Zheng ZX, Xi YY, Huang HG, Wu LL, Lin ZH (2001) NH_3 and HCl sensing characteristics of polyaniline nanofibers deposited on commercial ceramic substrates using interfacial polymerization. Phys Chem Commun 21:1–2

[19] Anitha G, Subramanian E (2005) Recognition and exposition of intermolecular interaction between CH_2Cl_2 and $CHCl_3$ by conducting polyaniline materials. Sens Actuators, B 107:605–615

[20] Xue H, Shen Z, Li C (2005) Improved selectivity and stability of glucose biosensor based on in situ electropolymerized polyaniline–polyacrylonitrile composite film. Biosens Bioelectron 20:2330–2334

[21] Chen J, Yang J, Yan X, Xue Q (2010) NH_3 and HCl sensing characteristics of poly-aniline nanofibers deposited on commercial ceramic substrates using inter-facial polymerization. Synth Met 160:2452–2458

[22] Wang N, Li J, Lv W, Feng J, Yan W (2015) Synthesis of polyaniline/TiO_2 composite with excellent adsorption performance on acid red G. RSC Adv 5:21132–21141

[23] Wang L, Zhang J, Wang A (2008) Removal of methylene blue from aqueous solution using chitosan-*g*-poly (acrylic acid)/montmorillonite superadsorbent nanocomposite. Colloids Surf A Physicochem Eng Asp 322:47–53

[24] Yang TH, Yi YG, Kim HS, Hong CY, Kim HB, Cho HY (2000) Mossbauer effect of the alkaline and alkaline earth metal nitroprusside powders. J Korean Phys Soc 37(3):290–294

[25] Buchs M, Daul CA, Manoharan PT, Schlapfer CW (2003) Density functional study of nitroprusside: mechanism of the photochemical formation and deactivation of the metastable states. Int J Quantum Chem 91:418–431

[26] Najar MH, Majid K (2015) Synthesis and characterization of nanocomposite of polythiophene with $Na_2[Fe(CN)_3(OH)(NO)C_6H_{12}N_4]$ H_2O: a potent material for EMI shielding applications. J Mater Sci Mater Electron 26:6458–6470

[27] Salem MA (2010) The role of polyaniline salts in the removal of direct blue 78 from aqueous solution: a kinetic study. React Funct Polym 70:707–714

[28] Naqash W, Majid K (2016) Synthesis, characterization and study of thermal, electrical and photocatalytical activity of nanocomposite of PANI with $[Co(NH_3)_4(C_{12}H_8N_2)]Cl_3{\cdot}5H_2O$ photoadduct. Chem Phys 478:118–125

[29] Shahabuddin S, Sarih NM, Ismail FH, Shahid MM, Huang NM (2015) Synthesis of chitosan grafted-polyaniline/Co_3O_4 nanotube nanocomposite and its photocatalytic activity toward methylene blue dye degradation. RSC Adv 5:83857–83867

[30] Farghali AA, Moussa M, Khedr MH (2010) Synthesis and characterization of novel conductive and magnetic nanocomposites. J Alloys Compd 98:499

[31] Rafiqi FA, Majid K (2016) Synthesis, characterization, photophysical, thermal and electrical properties of composite of polyaniline with zinc bis(8-hydroxyquinolate): a potent composite for electronic and optoelectronic use. RSC Adv 6:22016–22025

[32] Sen TK, Afroze S, Ang HM (2011) Equilibrium, kinetics and mechanism of removal of methylene blue from aqueous solution by adsorption onto pine cone biomass of pinus radiate. Water Air Soil Pollut 218:499–515

[33] Zhang Y, Wang W, Zhang J, Liu P, Wang A (2015) A comparative study about adsorption of natural palygorskite for methylene blue. Chem Eng J 262:390–398

[34] Shaibu SE, Adekola FA, Adegoke HI, Ayanda OS (2014) A comparative study of the adsorption of methylene blue onto synthesized nanoscale zero-valent iron-bamboo and manganese-bamboo composites. Materials 7:4493–4507

[35] Bai L, Li Z, Zhang Y, Wang T, Lu R, Zhou W, Gao H, Zhang S (2015) Synthesis of water-dispersible graphene-modified magnetic polypyrrole nanocomposite and its ability to efficiently adsorb methylene blue from aqueous solution. Chem Eng J 279:757–766

[36] Wang W, Ding Z, Cai M, Jian H, Zheng Z, Li F (2015) Synthesis and high-efficiency methylene blue adsorption of magnetic PAA/$MnFe_2O_4$ nanocomposites. Appl Surf Sci 346:348–353

[37] Xiao JD, Qiu LG, Jiang X, Zhu YJ, Ye S, Jiang X (2013) Magnetic porous carbons with high adsorption capacity synthesized by a microwave-enhanced high temperature ionothermal method from a Fe-based metal-organic framework. Carbon 59:372–382

[38] Rocher V, Bee A, Siaugue JM, Cabuit V (2010) J. Hazard. Mater. Dye removal from aqueous solution by magnetic alginate beads crosslinked with epichlorohydrin 178:434–439

[39] Ansari R, Mosayebzadeh Z (2011) Application of polyaniline as an efficient and novel adsorbent for azo dyes removal from textile wastewaters. Chem Pap 65:1–8

[40] Karthikaikumar S, Kartheikiyan M, Kumar KKS (2014) Removal of Congo red dye from aqueous solution by polyaniline–montmorrillonite composite. Chem Sci Rev Lett 2:606–614

[41] Zhang F, Lan J, Yang Y, Wei T, Tan R, Song W (2013) Adsorption behavior and mechanism of methyl blue on zinc oxide nanoparticles. J Nanopart Res 15:2034–2043

[42] Rafiqi FA, Majid K (2015) Removal of copper from aqueous solution using polyaniline and polyaniline/ferricyanide composite. J Environ Chem Eng 3:2492–2501

[43] Xia Y, Li T, Chen J, Cai C (2013) Polyaniline (skin)/polyamide 6 (core) composite fiber: preparation, characterization and application as a dye adsorbent. Synth Met 175:163–169

[44] Rehman MS-U, Kim I, Rashid N, Umer M, Sajid M, Han J-I (2016) Adsorption of brilliant green on biochar prepared from lignocellulosic bioethanol plant. Clean Soil Air Water 44(1):55–62

[45] Vimonses V, Lei S, Jin B, Chow CWK, Saint C (2009) Kinetic study and equilibrium isotherm analysis of Congo red adsorption by clay materials. Chem Eng J 148:354–364